Phase diagram of trivalent and pentavalent patchy particles

2012 J. Phys.: Condens. Matter 24 064113

(http://iopscience.iop.org/0953-8984/24/6/064113)

J. Phys.: Condens. Matter **24** (2012) 064113 (8pp) doi:10.1088/0953-8984/24/6/064113

Phase diagram of trivalent and pentavalent patchy particles

Flavio Romano[1], Eduardo Sanz[2], Piero Tartaglia[3] and Francesco Sciortino[3]

[1] Dipartimento di Fisica, Sapienza—Università di Roma, Piazzale Aldo Moro 5, 00185 Roma, Italy
[2] SUPA, School of Physics and Astronomy, University of Edimburgh, Mayfield Road, Edinburgh, UK
[3] Dipartimento di Fisica and CNR–ISC, Sapienza—Università di Roma, Piazzale Aldo Moro 5, 00185 Roma, Italy

Received 3 May 2011
Published 25 January 2012
Online at stacks.iop.org/JPhysCM/24/064113

Abstract
We compute the equilibrium phase diagram of two simple models for patchy particles with three and five patches in a very broad range of pressure and temperature. The phase diagram presents low-density crystal structures which compete with the fluid phase. The phase diagram of the five-patch model shows re-entrant melting, in analogy with the previously studied four-patch case, a metastable gas–liquid critical point and a stable, high-density liquid. The three-patch model shows a stable gas–liquid critical point and, in the region of temperatures where equilibration is numerically feasible, a stable liquid phase, suggesting the possibility that in this small valence model the liquid retains its thermodynamic stability down to the vanishing range limit.

(Some figures in this article are in colour only in the electronic version)

1. Introduction

Investigations of the collective behaviour of patchy colloidal particles [1–3] are expected to grow in the near future, when the newly synthesized colloidal particles with patterns of sticky patches on their surfaces will be produced in large quantities [4–6]. Recent developments in colloidal science are indeed starting to provide particles with specific directional interactions [7–11], opening the way to the study of structures (micelles [9], wires, sheets [12] or two- [11], and three-dimensional crystals) arising from their self-assembly. In addition to the experimental studies, several groups [13–20] are nowadays working on developing effective potentials for patchy colloids, with different levels of accuracy. Numerical and theoretical studies of these models are not only providing a wide picture of the possibilities offered by these particles but also revealing some unexpected novel phenomena arising from the possibility of controlling the potential asymmetry [13, 21–23]. A significant effort is in the direction of evaluating the phase diagram [13], the possible crystal structures [16], the competition with kinetic bottlenecks [18, 24] which bring the system into non-ergodic states (gels or glasses), as well as some fundamental problems such as the onset of gas–liquid criticality [13, 15, 23] or the essence of the gel state [24, 25].

One of the directions which is receiving significant attention is the investigation of the crystal structures in patchy colloids. This is not a coincidence, since colloidal crystals are expected to find application in several technological applications. Recent experimental [11] and numerical [26] studies have focused on the crystallization of two-patch particles in two dimensions in the exotic kagome structure. Several other studies [27–30] have been devoted to the possibility of self-assembling diamond crystal, one of the structures which is predicted to have an optimal photonic band gap in visible light [31]. In this specific case, the self-assembly of particles with four patches disposed on a tetrahedral geometry has been investigated. It has been shown that when the angular patch width is smaller than about 30°, the particles crystallize (in computer simulations) in a tetrahedral open structure, while for wider patches crystallization is pre-empted by the formation of an arrested state.

In this paper we investigate the phase diagram of particles with three and five patches, modelled via the Kern–Frenkel [32] potential. This potential, introduced originally to assess the dependence of the gas–liquid critical point on the

number, range and width of the patches, has been thoroughly investigated in recent years [21, 23, 26–28, 33, 34]. Within this model it is indeed possible to independently control, for each patch, the range and angular width, offering the possibility of investigating the different roles of these parameters in the self-assembly process. In addition, this model provides a good description of the interaction potential for the Janus and triblock Janus particles, recently investigated by the group of Granick [11], as shown in [26].

The results reported in this paper, combined with the previously published data for patchy particles with four patches [27, 28, 30], as well as with the well known tendency of six-patch particles to crystallize in a simple cubic crystal [35, 36], offer the possibility of extracting some general trends of the stability of the liquid phase with valence (the analogue of the previously investigated stability of the liquid phase with interaction range [37–39]). The results for the Kern–Frenkel model presented here (for a fixed angular width of the patches and a short range) suggest that a stable gas–liquid coexistence progressively emerges on reducing the valence. A stable liquid phase can indeed exist for three-patch particles down to very small temperatures, favoured by the absence of an open truly three-dimensional crystal of fully bonded particles. Finally, we provide an assessment of the role of the range in the stability of the liquid.

2. Model

We study the Kern–Frenkel [32] model for particles with three and five patches. In the first case, three directionally attractive sites (patches) are placed along the equator of a hard sphere. Each patch forms an angle of 120° with both the others. In the five-patch case, two additional patches are located on the north and south poles. A sketch of the particles is shown in figure 1. The two-body potential is written as a product of a square-well potential u_{SW} and a function that depends solely on the orientations of the patches (defined via the orientation of particle i, Ω_i):

$$u(\mathbf{r}_{ij}) = u_{\mathrm{SW}}(r_{ij}) f(\{\Omega_i, \Omega_j\}), \tag{1}$$

where

$$u_{\mathrm{SW}}(r_{ij}) = \begin{cases} \infty & r \leqslant \sigma \\ -u_0 & r \leqslant \sigma + \Delta \\ 0 & r \geqslant \sigma + \Delta. \end{cases} \tag{2}$$

The function $u_{\mathrm{SW}}(r_{ij})$ is a square-well potential of attractive range Δ and depth u_0, while the modulating function f is defined as follows. Let $\hat{\mathbf{u}}_i^{\alpha}$ be the normalized vector that, starting from the centre of the particle i, points towards the interaction site labelled by α (ranging from 1 to the number of patches) on its surface, and $\hat{\mathbf{r}}_{ij}$ be the normalized vector connecting the centres of particles i and j. The function f reads

$$f(\Omega_i, \Omega_j) = \begin{cases} 1 & \text{if} \begin{cases} \hat{\mathbf{r}}_{ij} \cdot \hat{\mathbf{u}}_i^{\alpha} > \cos(\theta_{\max}) & \text{for any } \alpha \\ \text{and} \\ \hat{\mathbf{r}}_{ji} \cdot \hat{\mathbf{u}}_j^{\alpha} > \cos(\theta_{\max}) & \text{for any } \alpha \end{cases} \\ 0 & \text{otherwise.} \end{cases} \tag{3}$$

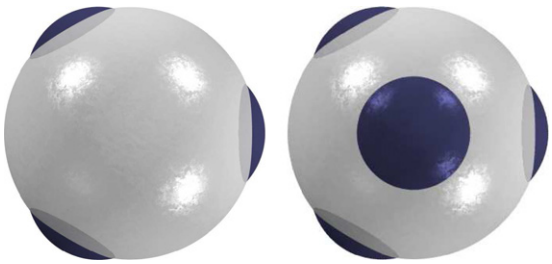

Figure 1. Graphical representation of a three-patch particle (left) and a five-patch particle (right) as described by the Kern–Frenkel model. The hard sphere is drawn in white while the attractive patches are in blue.

Then, to form a bond, two particles must be within the square-well range and each particle must have a patch that forms an angle smaller than a maximum angle $\theta_{\max}$ with the vector connecting the centres of the two particles. In this study, for both the three-patch model and the five-patch model the radial interaction range δ is fixed to 0.12σ and $\cos(\theta_{\max})$ is fixed at 0.92. This choice of δ and $\theta_{\max}$ ensures that each patch can be involved in no more than a single bond [40], so that the ground state potential energy per particle is fixed at $u_{\mathrm{gs}} = -Mu_0/2$, with M the valence of the model (i.e. the number of patches).

In the following, we use reduced units with $\sigma = 1$ and $u_0 = 1$, temperature T is measured in units of u_0/k_{B} (where k_{B} is the Boltzmann constant), number density ρ in units of σ^{-3} and pressure P in units of u_0/σ^3.

3. Numerical calculations of phase diagrams

The numerical procedure for computing phase diagrams of anisotropic potentials is a well-established one; many examples of phase diagrams of anisotropic particles can be found in the literature [28, 36, 41, 42]. As in previous work, we refer to the review of Vega *et al* [43] for the details of the computations; here we shall only give a list of the procedures undertaken.

Computation of phase diagrams requires a combination of techniques, starting with a guess of the possible thermodynamic phases that will be found to be stable. Although several techniques aimed at guessing the stable crystal structures at low temperatures have been recently proposed [44–46], due to the simplicity of the model studied here we selected the crystal structures to be investigated with simple considerations based on the symmetry of the model and the limiting case at high temperature and pressure. Once a series of thermodynamic phases to test is found, one has to compute their chemical potential to find some coexistence state points. This can be accomplished in various ways, all based on the integration of a partial derivative of the free energy along a thermodynamic path, be it physical (i.e. change in temperature or pressure) or non-physical (gradually coupling the system to a Hamiltonian of known free energy). Once a coexistence point is found between phases I and II (i.e. $\mu_{\mathrm{I}}(P_{\mathrm{coex}}, T_{\mathrm{coex}}) = \mu_{\mathrm{II}}(P_{\mathrm{coex}}, T_{\mathrm{coex}})$), one can use Gibbs–Duhem integration to follow the coexistence lines [47].

In this paper, we computed the chemical potential of the fluid phase using thermodynamic integration starting from high temperature and gradually lowering the temperature at fixed βP, $\beta = 1/(k_B T)$ being the inverse temperature. When $\beta \to 0$, the chemical potential tends to that of the hard-sphere (HS) model. By using the Carnahan–Starling approximation [48], we take

$$\beta\mu_{\rm HS} = \log(\rho) - 1 + \frac{4\eta - 3\eta^2}{(1-\eta)^2} + Z_{\rm HS}, \tag{4}$$

where η is the packing fraction and $Z_{\rm HS} = \beta P_{\rm HS}/\rho$ is the Carnahan–Starling compressibility factor for hard spheres. As

$$\left.\frac{\partial\beta\mu}{\partial\beta}\right|_{\beta P} = u \tag{5}$$

it is possible to compute $\beta\mu$ as

$$\beta\mu(\beta, \beta P) = \beta_0\mu(\beta_0, \beta_0 P_0) + \int_{\beta_0}^{\beta} {\rm d}\beta' \langle u\rangle_{\beta', \beta' P}, \tag{6}$$

where the integrand can be evaluated with numerical simulations in the NPT ensemble. Starting from the high-temperature limit ($\beta_0 = 1$ is sufficient in our case), we use the following expression:

$$\beta\mu(\beta, \beta P) = \beta_0(\mu_{\rm HS} + \langle u\rangle_{\beta_0, \beta_0 P}) + \int_{\beta_0}^{\beta} {\rm d}\beta' \langle u\rangle_{\beta', \beta' P}; \tag{7}$$

we have checked that this expression gives very reliable results by simulating a few state points at low T in the $N\mu T$ ensemble.

To compute the free energies of all the crystal structures studied (except for the planar crystal of the three-patch model) we have used a standard Frenkel–Ladd [49] procedure for hard-core particles extended to anisotropic potentials. This procedure consists in coupling the system to an Einstein crystal of known free energy that has the same symmetry as the model. We refer the reader to [28, 43] for the details of the procedure, pointing out that we used as a reference system an Einstein crystal with fixed centre of mass with a D_{3h}-symmetric Hamiltonian (see equation (A.6) in the appendix) for both models.

We used as starting configurations for the Frenkel–Ladd technique equilibrium configurations of the crystals generated in constant P simulations, treating each of the box directions independently; this is particularly important, as discussed in [41], to allow the pressure to equilibrate properly along the different directions in the lattice.

In the case of the three-patch model, one possible fully bonded configuration is composed of independent (not bonded) planes floating in three dimensions. This makes it impossible to use the Frenkel–Ladd procedure since the reference free energy diverges, and a different reference Hamiltonian has to be used. Very recently, a clever modification of the Frenkel–Ladd procedure has been proposed by Schilling and Schmid [50] that allows one to overcome this problem. The procedure they propose is essentially the same as the Frenkel–Ladd procedure, but they use a reference Hamiltonian that, contrary to the Einstein crystal Hamiltonian, has the property of providing a bounded reference free energy. This is made possible by a choice of the reference Hamiltonian and *ad hoc* Monte Carlo moves. Here we use a straightforward extension to their reference Hamiltonian, applicable to thermal and anisotropic systems. Our reference Hamiltonian is split into two parts, one that constrains the translational degrees of freedom ($H_{\rm ref}^{\rm tras}$) and another one that constrains the orientational degrees of freedom ($H_{\rm res}^{\rm or}$). $H_{\rm ref}^{\rm tras}$ is the reference Hamiltonian introduced in [50],

$$H_{\rm ref}^{\rm tras}(\epsilon) = \epsilon \sum_{i=0}^{N} \min\{(|\mathbf{r}_i - \mathbf{r}_{0,i}|/r_{\rm c} - 1), 0\}, \tag{8}$$

where $\mathbf{r}_i$ is the position of particle i and $\mathbf{r}_{0,i}$ is the position of particle i in an equilibrium configuration of the system. $H_{\rm ref}^{\rm or}$ (see equation (A.6) in the appendix) is a Hamiltonian with the same symmetry as the model [43]. In the reference system the orientational and translational degrees of freedom are totally decoupled, so that the reference free energy is the sum of the orientational contribution, known either analytically or by Monte Carlo integration [43], and the translational free energy associated with the Schilling and Schmid Hamiltonian that reads

$$\beta f = \log(\rho) - 1 - \log\left[1 + \frac{(4/3)\pi r_{\rm c}^3}{V} g(\beta\epsilon)\right], \tag{9}$$

$$g(\beta\epsilon) = 3(\beta\epsilon)^3(e^{\beta\epsilon} - 1 - (\beta\epsilon) - (\beta\epsilon)^2/2 - (\beta\epsilon)^3/3). \tag{10}$$

A more detailed explanation of the free energy calculations can be found in the appendix.

The gas–liquid coexistence lines were computed with the Gibbs ensemble simulation technique [51]. A detailed study of the critical behaviour of both models can be found in [40].

4. Crystal structures

In the light of results of similar models [28], it is expected that stable crystal structures at low T are limited to fully bonded structures. The particle geometry thus greatly restricts the possible lattices, which are just a few. In the three-patch case, we have been able to identify three different fully bonded structures: (i) a collection of independent planes, each formed by particles sitting in a two-dimensional hexagonal lattice (figure 2(a)), forming free hexagonal planes (FHP); (ii) a crystal made of inter-penetrating hexagonal planes (IHP) (figure 2(b)); and (iii) a fully bonded FCC structure (figure 2(c)). In the perfect FCC lattice full bonding is possible only if the patches are wide enough ($\cos\theta \lesssim 0.95$) to account for the fact that the local FCC environment is not compatible with the patch arrangement. This causes the FCC to be distorted (one of the cell edges is ∼5% larger than the other two), since the local environment tends to rearrange to better reflect the particles' symmetry. At high T, we expect that the FCC fully bonded structure converts to an orientationally disordered (plastic) FCC phase (FCC-p). In the five-patch model, besides the FCC, the only fully bonded structure we have been able to identify is a structure of

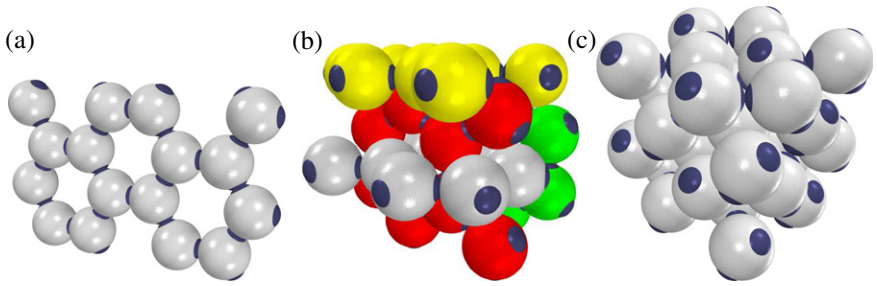

Figure 2. Schematic representation of the crystals examined in the case of the three-patch model: (a) free hexagonal planes (FHP) (only one plane is shown), (b) inter-penetrating hexagonal planes (IHP) (different planes are shaded differently for clarity), and (c) fully bonded FCC. The rotationally disordered (plastic) phase, stable at high T, is not shown. For a better visualization of the structure, particles in the IHP phase are coloured according to the plane they belong to.

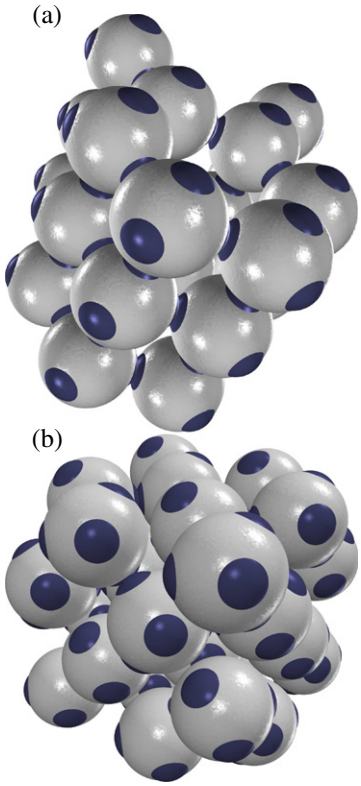

Figure 3. Schematic representation of the bonded hexagonal planes (BHP) (a) and of the fully bonded FCC model (b). The plastic FCC-p, stable at high T, is not shown.

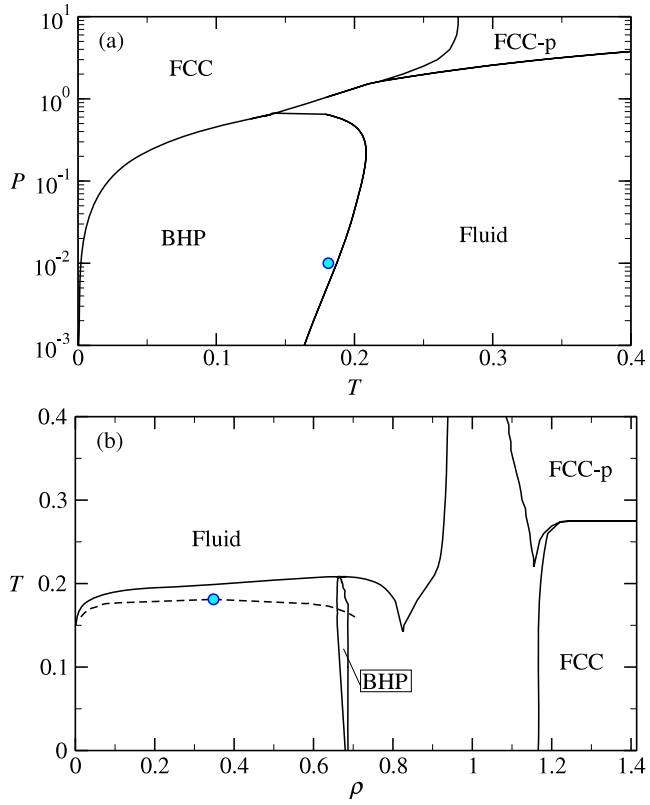

Figure 4. Phase diagrams of the five-patch model in the (a) P–T and (b) T–ρ representations. The critical point (cyan circle) is metastable with respect to the planar phase. The region where the coexistence lines are dashed in both panels corresponds to the stability region of a high-density liquid, and since its equilibration is hard our results have a significant error, of the order of 10–15% in T in that area.

bonded hexagonal planes (BHP), joined by the patches located on the particle poles (figure 3). Due to the short-range, square-well-like interaction, all fully bonded crystals have the same free energy at $T = 0$ and $P = 0$, where the entropic and volume contributions are zero. At $T = 0$ and positive P, the denser phase always has the lowest free energy, being favoured by the PV term in the chemical potential. As a comment, we stress that in the case of patchy models, the ground state crystal structures can have densities significantly smaller than the close-packed structures that characterize the phase diagram of spherically interacting colloids. Also in this case the stable phase at high T and P is the orientationally disordered FCC-p.

5. Results

Figure 4(a) shows the phase diagram in P–T for the five-patch model. The stacked planar structure (figure 3) is the stable phase at low T and P, turning into the FCC structure at high P. At high T and low P, the fluid phase is the most stable. The fluid–BHP coexistence is re-entrant, i.e. increasing P for $T \approx 0.2$ the system goes from a fluid to a crystal and then, upon further increasing P, it melts back into a high-density fluid phase, before transforming into the FCC phase, the stablest at

high P. According to the Clapeyron equation, $\mathrm{d}P/\mathrm{d}T$ along the coexistence line provides the ratio of the differences in entropy ΔS and volume ΔV of the two coexisting phases. At the onset of the re-entrance, the crystal and the fluid have the same density. In the anomalous region ($\mathrm{d}P/\mathrm{d}T < 0$), the fluid density is higher than the crystal density and the fluid will expand on crystallizing. The fluid–crystal re-entrance has been already observed in the case of tetravalent models [27–29, 52] and appears thus to be a generic feature when the fluid coexists with an open crystal, although the possibility of observing such re-entrance as a stable thermodynamic phenomenon may depend on the potential parameters [28] or on the presence of other crystal structures. The gas–liquid critical point, for the present interaction range, is slightly metastable, and it is located well within the re-entrant region. Hence, re-entrance may involve two fluids or one gas and one liquid phase which sandwich the crystal phase.

The T–ρ phase diagram, more relevant to colloidal science, is shown in figure 4(b). The BHP crystal is stable at $\rho \approx 0.68$. The re-entrance manifests itself in the dip in the stability of the fluid (liquid) phase around $\rho \approx 0.85$. The liquid is here denser than the open crystal and less dense than the FCC structure. It would be interesting to explore the dynamics of the liquid at this density to see if it already shows the signature of glassy behaviour, as this situation is similar to the eutectic point in mixtures of elements that have a single chemical composition that solidifies at a lower temperature than any other composition. In the region where the high-density fluid is stable, the bonding is so extensive that it is very hard to reach equilibrium in a computer simulation. Indeed, at $T = 0.15$ and $\rho \approx 0.35$, the energy is lower than $-2.35u_0$, i.e. each particle is involved on average in more than 4.7 attractive interactions.

The phase diagram of the three-patch model is reported in figure 5. The first observation is that we could not determine whether the free hexagonal plane phase has a region of stability: it is indeed more stable that the other fully bonded structures at low T and P, but since equilibration of the liquid is impossible at $T \leqslant 0.07$ we could not compute either the IHP–liquid or the FHP–liquid coexistence lines; for $T > 0.07$ the liquid is more stable than the FHP phase at the pressures shown. The intermediate-density IHP structure does have a region of stability at low T, before becoming less stable than the fully bonded FCC at higher pressures. The new element here is the absence of a stable crystal phase at low T and P. The fluid separates into a gas and a liquid phase at the critical point but the liquid phase always remains stable. This is very uncommon and it is a genuine feature of low valence systems. In the T–ρ phase diagram (figure 5(b)) this appears as a region where the liquid can be cooled down to vanishing T without encountering any coexistence lines. While all the crystal–crystal coexistence curves can be traced down to $T = 0$, since no structural changes take place on cooling and the crystals have already approached the ground state, the crystal–liquid coexistence can be only calculated down to the lowest temperature ($T \approx 0.07$) at which the liquid can be properly equilibrated. Hence, we cannot provide a definitive proof that the liquid state is stable down to $T = 0$. Nevertheless, it is important to notice that at $T \approx 0.07$ the liquid is essentially

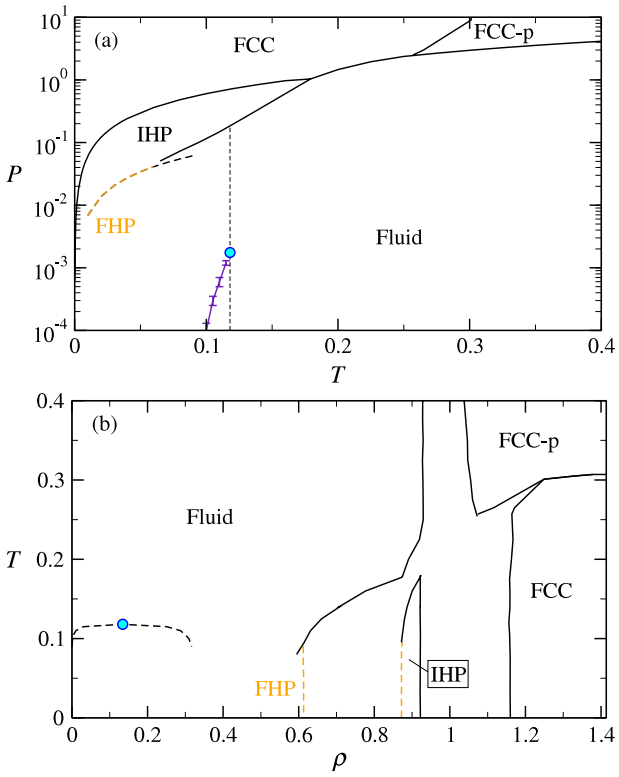

Figure 5. Phase diagrams of the three-patch model in the (a) P–T and (b) T–ρ representations. The critical point (cyan circle) and gas–liquid coexistence are stable. The label for the FHP phase is indicated via a light colour to call attention to the impossibility of determining its coexistence line with the liquid. The light coloured dashed line indicates the coexistence between the IHP and FHP phases, which could be metastable with respect to the liquid phase. There are wide regions in P (a) and ρ (b) where the liquid can be cooled down to a very low temperature without encountering crystallization or phase separation.

fully bonded [13], i.e. it has a potential energy comparable to that of the crystals. The majority of the driving force for crystallization would thus arise from the ΔS and $P\Delta V$ terms in the chemical potential. Since $\Delta V = \frac{\rho_{\mathrm{xt}} - \rho_{\mathrm{liquid}}}{\rho_{\mathrm{xt}}\rho_{\mathrm{liquid}}} \approx 1$ and $P \approx 10^{-2}$–10^{-1}, a significant contribution to the stabilization of the fluid phase for low P must arise from the entropic term, possibly related to the logarithm of the number of different fully bonded disordered configurations [30, 53]. Figure 6 shows the two hypothetical possibilities for the low T behaviour, depending on the stability of the liquid phase with respect to the FHP phase. In the first case, there is a triple point FHP–IHP–liquid and a region of stability for the FHP phase. In the second case, the FHP is always metastable with respect to the liquid phase and the only equilibrium coexistence line is between the IHP phase and the liquid.

6. Discussion and conclusions

The models we have studied represent only one of the possible distributions of patches on the particle surface. The choice has been made by selecting the locations that maximize the particles' symmetry. In this respect, the choice we have

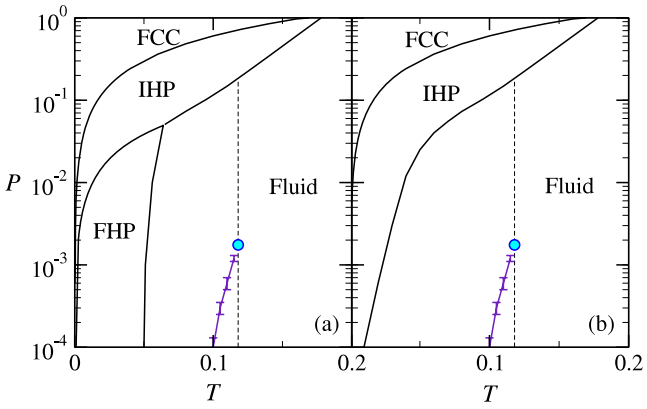

Figure 6. Hypothetical representation of the low T region of the phase diagram for the three-patch model. In (a) we assume that the FHP phase is more stable than the liquid for very low T and thus a triple point IHP–FHP–liquid is present. In (b) we assume that the FHP phase is never more stable than the liquid phase and hence the relevant low-T coexistence line is that between the IHP phase and the liquid.

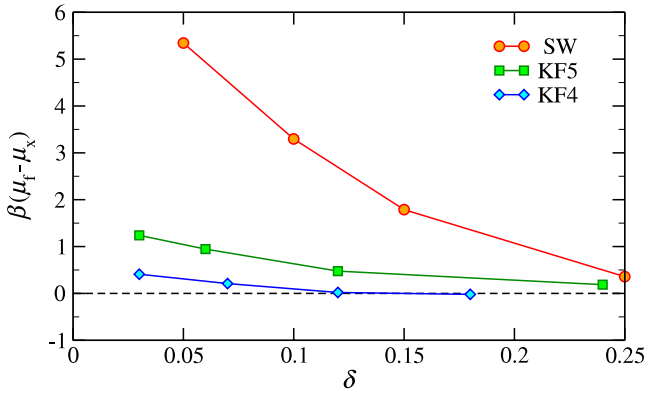

Figure 7. The driving force for crystal formation at the critical point as a function of the interaction range for a fixed angular width $\cos(\theta) = 0.92$ for models with four (KF4) and five (KF5) patches and the square-well (SW) model. Note that the case of three patches cannot be drawn, since there is no competing crystal at the critical point (that is, $\beta(\mu_f - \mu_x)$ is always negative). A clear trend with the valence is shown, with higher valences favouring the crystal structures.

made is the one that favours crystal formation, since fully bonded crystals can only be made by selecting structures compatible with the particles' symmetry. It is thus interesting to compare the stability of the liquid phase for models with a different number of equally sized patches. By reducing the number of patches one also progressively reduces the fraction of surface which is prone to bonding. Such a decrease lowers the gas–liquid critical temperature [13, 25, 40], but also affects the melting temperature. For a model of triblock Janus particles [34], it has been suggested that reducing the coverage might act similarly to the reduction of the range in spherically symmetric potentials [37–39]. To provide a complete picture of the phenomenon, we have evaluated the driving force for crystal formation at the gas–liquid critical point, defined as the difference in the fluid and crystal chemical potentials $\beta(\mu_f - \mu_x)$ (where $\beta = 1/(k_B T)$) for several values of the interaction range. The data are reported in figure 7, together with the corresponding data for the square-well potential and the four-patch model, reproduced from [27]. In the case of three patches we could not compute $\beta(\mu_{fluid} - \mu_{xt})$, since the fluid–solid coexistence line could not be extended to low temperatures. Figure 7 shows a clear trend in the direction of a progressive stabilization of the liquid phase on decreasing the valence. One contribution clearly comes from the fact that on decreasing the valence, the critical point emerges when the bonding becomes more pronounced. Indeed, in small valence systems, the bond probability at the critical point acts as a valence-dependent scaling variable [40] and its value increases on decreasing the valence. The more extensive bonding at the critical point which characterizes the small valence systems thus decreases the energetic driving force towards crystallization. The critical pressure is also strongly dependent on the valence, decreasing on decreasing valence [54, 55]. Hence, also the PV term in the chemical potential that favours the crystals becomes less and less effective. In this respect, the results reported in figure 7 do suggest that for valence three (and perhaps for binary mixtures with average valence smaller than three [55, 56]) the liquid retains its thermodynamic stability down to the vanishing range limit, a possibility that has recently been theoretically discussed [57].

Acknowledgments

We acknowledge support from ERC-226207-PATCHYCOLLOIDS and ITN-COMPLOIDS. ES is financed by a Marie Curie I-E fellowship. PT acknowledges support from MIUR-PRIN.

Appendix. Details for the free energy of the planar crystal

In this section, we will give detailed results regarding the calculation of the free energy of the FHP phase at a particular state point. We believe that this is useful, since the Frenkel–Ladd technique is not applicable to this structure since the reference free energy would diverge due to the motion of the planes as a whole. We warn the reader that the following discussion requires familiarity with [43] and [50].

Free energy calculations are based on thermodynamic integration from a system with known free energy. Possibly, this can be done in several steps, for example computing the free energy at a particular state point and then integrating its derivative along a thermodynamic path. We will summarize in what follows the procedure to compute the free energy of the free hexagonal planar phase for the Kern–Frenkel model with three patches introduced in the text.

The reduced free energy per particle βf along an isotherm can be recovered by computing its value at a particular density ρ_0 and then integrating the equation of state $P(\rho)$ at that T. First of all, we start a series of NPT simulations (independently controlling the length of the simulation box in the three directions) at $T = 0.05$ (a T at which bond breaking events do not take place) and varying P to recover the equation of state. We then select an intermediate value of the density at which to perform the calculation of the free energy: we

select $\rho_0 = 0.56$, corresponding to $P = 0.04$. We use the final configuration of our run at $P = 0.04$ as a reference configuration for the Schilling–Schmid technique [50], to make sure that it is a representative configuration at the selected density. We note that we have carefully checked that the pressure had equilibrated along all three sides of the simulation box.

Our discussion requires an explanation of how we define the orientation of the particles. Although other choices are equally valid, the treatment has to be changed accordingly. We define two perpendicular unit vectors, $\hat{\mathbf{a}}$ and $\hat{\mathbf{b}}$, so that the unit vectors identifying the three patches are defined as follows:

$$\hat{\mathbf{p}}_1 = \hat{\mathbf{a}}, \tag{A.1}$$

$$\hat{\mathbf{p}}_2 = \frac{1}{2}\hat{\mathbf{a}} + \frac{\sqrt{3}}{2}\hat{\mathbf{b}}, \tag{A.2}$$

$$\hat{\mathbf{p}}_3 = -\frac{1}{2}\hat{\mathbf{a}} + \frac{\sqrt{3}}{2}\hat{\mathbf{b}}. \tag{A.3}$$

To compute the absolute value of the free energy of our system at fixed T and ρ (0.05 and 0.56, respectively), following [50] we couple our system with a reference system of known free energy whose Hamiltonian reads

$$H_{\mathrm{ref}}(\epsilon) = H_{\mathrm{ref}}^{\mathrm{tras}}(\epsilon) + H_{\mathrm{ref}}^{\mathrm{or}}(\epsilon), \tag{A.4}$$

where

$$H_{\mathrm{ref}}^{\mathrm{tras}}(\epsilon) = \epsilon \sum_{i=0}^{N} \min\{(|\mathbf{r}_i - \mathbf{r}_{0,i}|/r_{\mathrm{c}} - 1), 0\} \tag{A.5}$$

and

$$H_{\mathrm{ref}}^{\mathrm{or}}(\epsilon) = \epsilon \sum_{i=0}^{N} (\sin^2 \psi_i^{\mathrm{a}} + \sin^2 \psi_i^{\mathrm{b}}), \tag{A.6}$$

where ψ_i^{a} (ψ_i^{b}) is the minimum angle formed by the vector $\hat{\mathrm{a}}$ ($\hat{\mathrm{b}}$) of particle i in the reference configuration and the vectors $\hat{\mathrm{a}}$ and ($\hat{\mathrm{b}}$) of particle i along the simulation.

The free energy of such a system can be decoupled into a translational and an orientational part. The expression for the translational part, provided in [50], is

$$\beta f_{\mathrm{ref}}^{\mathrm{tras}} = \log(\rho) - 1 - \log\left[1 + \frac{(4/3)\pi r_{\mathrm{c}}^3}{V} g(\beta\epsilon)\right], \tag{A.7}$$

where

$$g(\beta\epsilon) = 3(\beta\epsilon)^3(\mathrm{e}^{\beta\epsilon} - 1 - (\beta\epsilon) - (\beta\epsilon)^2/2 - (\beta\epsilon)^3/3). \tag{A.8}$$

The orientational reference free energy $\beta f_{\mathrm{ref}}^{\mathrm{or}}$ can be computed via a Monte Carlo integration of the following equation:

$$\beta f_{\mathrm{ref}}^{\mathrm{or}} = \frac{1}{8\pi^2} \int \mathrm{d}\psi\, \mathrm{d}\phi\, \mathrm{d}\theta \cos\theta \exp\{-\beta H_{\mathrm{ref}}^{\mathrm{or}}(\epsilon)\} \tag{A.9}$$

where ϕ, ψ and θ are the Euler angles.

The free energy of our reference system is thus $\beta f_{\mathrm{ref}} = \beta f_{\mathrm{ref}}^{\mathrm{tras}} + \beta f_{\mathrm{ref}}^{\mathrm{or}}$.

At this point, we introduce a mixed Hamiltonian H' which is the sum of the Hamiltonian under investigation H, the Kern–Frenkel Hamiltonian in our case, and the reference Hamiltonian $H_{\mathrm{ref}}(\epsilon)$. The quantity ϵ in the equations (A.5) and (A.6) thus controls the relative role amplitude of the reference Hamiltonian with respect to the unperturbed Kern–Frenkel Hamiltonian. By varying ϵ one can gradually move from a system in which the presence of H is undetectable when ϵ is very large to a system where the presence of H_{ref} is undetectable when ϵ is very small. If we choose a value of ϵ, ϵ_{max}, such that the presence of H is undetectable, we can compute the free energy of the system with Hamiltonian $H'(\epsilon_{\mathrm{max}})$ as

$$\beta f'(\epsilon_{\mathrm{max}}) = \beta f_{\mathrm{ref}}(\epsilon_{\mathrm{max}}) + \langle H \rangle_{\epsilon_{\mathrm{max}}}, \tag{A.10}$$

where $\langle H \rangle_{\epsilon_{\mathrm{max}}}$ is the ensemble average of the contribution to the potential energy of a system with Hamiltonian $H'(\epsilon_{\mathrm{max}})$ due to H.

The free energy difference Δf between a system with Hamiltonian $H'(\epsilon_{\mathrm{max}})$ and a system with Hamiltonian $H'(\epsilon = 0)$ can be found by integrating the free energy derivative with respect to ϵ:

$$\beta \Delta f = \int_0^{\epsilon_{\mathrm{max}}} \left\langle \frac{\mathrm{d}H'}{\mathrm{d}\epsilon} \right\rangle_{N,V,T,\epsilon} \mathrm{d}\epsilon, \tag{A.11}$$

where by derivation one obtains

$$\left\langle \frac{\mathrm{d}H'}{\mathrm{d}\epsilon} \right\rangle_{N,V,T,\epsilon} = N[\langle \min\{0, 1 - |\mathbf{r}_i - \mathbf{r}_{0,i}|/r_{\mathrm{c}}\} \rangle_{N,V,T,\epsilon} + \langle \sin^2 \psi_i^{\mathrm{a}} + \sin^2 \psi_i^{\mathrm{b}} \rangle_{N,V,T,\epsilon}]. \tag{A.12}$$

The integrand on the right-hand side of equation (A.11) can be found by running several simulations of a system with Hamiltonian H' at several values of ϵ until the value of the integral converges. As discussed in [50], special Monte Carlo moves (for example exchange of particle identity) have to be implemented to ensure convergence. Although such moves are not needed in the case of a three-dimensional crystal, they are important when the particles diffuse, which is the case for the FHP phase along one direction.

The final free energy of the system can be recovered as follows:

$$\beta f = \beta f'_{\mathrm{ref}}(\epsilon_{\mathrm{max}}) + \beta f_{\mathrm{ref}}^{\mathrm{or}} + \Delta f. \tag{A.13}$$

As a reference for further studies, we detail here the calculation of the free energy of the FHP crystal at $T = 0.05$ and $\rho = 0.56$, corresponding to $P = 0.04$ in reduced units. We run twenty simulations of the system with Hamiltonian H' with values of ϵ logarithmically spaced between 0.01 and 300. We use $\epsilon_{\mathrm{max}} = 300$, $r_{\mathrm{c}} = 1.5\sigma$ and $N = 256$ particles and obtain

$$\beta f_{\mathrm{ref}}^{\mathrm{tras}} = -5973.80, \tag{A.14}$$

$$\beta f_{\mathrm{ref}}^{\mathrm{or}} = 14.11, \tag{A.15}$$

$$\beta u = -30.00, \tag{A.16}$$

$$\Delta f = -5968.36. \tag{A.17}$$

Thus, the free energy of the FHP at $T = 0.05$, $\rho = 0.56$ is $\beta f = -21.29$. The corresponding value of the chemical

potential at $T = 0.05$, $P = 0.04$ is thus $\beta\mu = \beta f + \beta P/\rho = -19.86$. The value of the chemical potential along the $T = 0.05$ isotherm can be recovered by integration of the enthalpy as shown in [43]. The expected precision of the final value of βf is of the order of $\pm 0.04 k_B T$.

References

[1] Glotzer S C and Solomon M J *Nat. Mater.* **6** 557
[2] Pawar A B and Kretzschmar I 2010 *Macromol. Rapid Commun.* **31** 150
[3] Bianchi E, Blaak R and Likos C N 2011 *Phys. Chem. Chem. Phys.* **13** 6397
[4] Manoharan V N, Elsesser M T and Pine D J 2003 *Science* **301** 483
[5] Zerrouki D, Rotenberg B, Abramson S, Baudry J, Goubault C, Leal-Calderon F, Pine D J and Bibette J 2006 *Langmuir* **22** 57
[6] Zhang G, Wang D and Möhwald H 2005 *Nano Lett.* **5** 143
[7] Yethiraj A and van Blaaderen A 2003 *Nature* **421** 513
[8] Kraft D J, Groenewold J and Kegel W K 2009 *Soft Matter* **5** 3823
[9] Jiang S, Chen Q, Tripathy M, Luijten E, Schweizer K S and Granick S 2010 *Adv. Mater.* **22** 1060
[10] Hermans T M, Broeren M A C, Gomopoulos N, van der Schoot P, van Genderen M H P, Sommerdijk N A J M, Fytas G and Meijer E W 2009 *Nat. Nanotechnol.* **4** 721
[11] Chen Q, Bae S C and Granick S 2011 *Nature* **469** 381
[12] Tang Z, Zhang Z, Wang Y, Glotzer S C and Kotov N A 2006 *Science* **314** 274
[13] Bianchi E, Largo J, Tartaglia P, Zaccarelli E and Sciortino F 2006 *Phys. Rev. Lett.* **97** 168301
[14] Tavares J M, Teixeira P I C and da Gama M M T 2009 *Mol. Phys.* **107** 453
[15] Tavares J M, Teixeira P I C and da Gama M M T 2009 *Phys. Rev.* E **80** 021506
[16] Doppelbauer G, Bianchi E and Kahl G 2010 *J. Phys.: Condens. Matter* **22** 104105
[17] Wilber A W, Doye J P K, Louis A A, Noya E G, Miller M A and Wong P 2007 *J. Chem. Phys.* **127** 085106
[18] Doye J P K, Louis A A, Lin I, Allen L R, Noya E G, Wilber A W, Kok H C and Lyus R 2007 *Phys. Chem. Chem. Phys.* **9** 2197
[19] Zhang Z, Keys A S, Chen T and Glotzer S C 2005 *Langmuir* **21** 11547
[20] Ding Y and Kroger M 2009 *Macromolecules* **42** 576
[21] Sciortino F, Giacometti A and Pastore G 2009 *Phys. Rev. Lett.* **103** 237801
[22] Russo J and Sciortino F 2010 *Phys. Rev. Lett.* **104** 195701
[23] Russo J, Tavares J M, Teixeira P I C, Telo da Gama M M and Sciortino F 2011 *Phys. Rev. Lett.* **106** 085703
[24] Zaccarelli E 2007 *J. Phys.: Condens. Matter* **19** 323101
[25] Zaccarelli E, Buldyrev S V, La Nave E, Moreno A J, Saika-Voivod I, Sciortino F and Tartaglia P 2005 *Phys. Rev. Lett.* **94** 218301
[26] Romano F and Sciortino F 2011 *Soft Matter* **7** 5799–804
[27] Romano F, Sanz E and Sciortino F 2009 *J. Phys. Chem.* B **113** 15133
[28] Romano F, Sanz E and Sciortino F 2010 *J. Chem. Phys.* **132** 184501
[29] Noya E G, Vega C, Doye J P K and Louis A A 2010 *J. Chem. Phys.* **132** 234511
[30] Romano F, Sanz E and Sciortino F 2011 *J. Chem. Phys.* **134** 174502
[31] Maldovan M and Thomas E L 2004 *Nat. Mater.* **3** 593
[32] Kern N and Frenkel D 2003 *J. Chem. Phys.* **118** 9882
[33] Giacometti A, Lado F, Largo J, Pastore G and Sciortino F 2009 *J. Chem. Phys.* **131** 174114
[34] Giacometti A, Lado F, Largo J, Pastore G and Sciortino F 2010 *J. Chem. Phys.* **132** 174110
[35] Liu H, Kumar S K and Douglas J F 2009 *Phys. Rev. Lett.* **103** 018101
[36] Noya E G, Vega C, Doye J P K and Louis A A 2007 *J. Chem. Phys.* **127** 054501
[37] Anderson V J and Lekkerkerker H N W 2002 *Nature* **416** 811
[38] Tejero C F, Daanoun A, Lekkerkerker H N W and Baus M 1994 *Phys. Rev. Lett.* **73** 752
[39] Hagen M H J, Meijer E J, Mooij G C A M, Frenkel D and Lekkerkerker H N W 1993 *Nature* **365** 425
[40] Foffi G and Sciortino F 2007 *J. Phys. Chem.* B **33** 9702
[41] Noya E G, Conde M M and Vega C 2008 *J. Chem. Phys.* **129** 104704
[42] Li X, Gunton J and Chakrabarti A 2009 *J. Chem. Phys.* **131** 115101
[43] Vega C, Sanz E, Abascal J L F and Noya E G 2008 *J. Phys.: Condens. Matter* **20** 153101
[44] Filion L, Marechal M, van Oorschot B, Pelt D, Smallenburg F and Dijkstra M 2009 *Phys. Rev. Lett.* **103** 188302
[45] Gottwald D, Likos C N, Kahl G and Löwen H 2004 *Phys. Rev. Lett.* **92** 068301
[46] Pauschenwein G J and Kahl G 2008 *Soft Matter* **4** 1396
[47] Kofke D A 1993 *Mol. Phys.* **78** 1331
[48] Carnahan N F and Starling K E 1969 *J. Chem. Phys* **51** 635
[49] Frenkel D and Ladd A J C 1984 *J. Chem. Phys.* **81** 3188
[50] Schilling T and Schmid F 2009 *J. Chem. Phys.* **131** 231102
[51] Panagiotopoulos A Z 1987 *Mol. Phys.* **61** 813
[52] Vega C and Monson P 1998 *J. Chem. Phys.* **109** 9938
[53] Moreno A J, Buldyrev S V, La Nave E, Saika-Voivod I, Sciortino F, Tartaglia P and Zaccarelli E 2005 *Phys. Rev. Lett.* **95** 157802
[54] Sciortino F and Tartaglia P 2010 *J. Phys.: Condens. Matter* **22** 104108
[55] de las Heras D, Tavares J M and Telo da Gama M M 2011 *Soft Matter* **7** 5615–26
[56] Bianchi E, Tartaglia P, La Nave E and Sciortino F 2007 *J. Phys. Chem.* B **111** 11765
[57] Charbonneau P and Frenkel D 2007 *J. Chem. Phys.* **126** 054501